ACS APPLIED MATERIALS & INTERFACES

Research Article

www.acsami.org

Antimicrobial and Osteogenic Properties of Silver-Ion-Implanted Stainless Steel

Hui Qin,[†,‡] Huiliang Cao,[§,‡] Yaochao Zhao,[†] Guodong Jin,[§] Mengqi Cheng,[†] Jiaxin Wang,[†] Yao Jiang,[†] Zhiquan An,[†] Xianlong Zhang,*[,†] and Xuanyong Liu*[,§]

[†]Department of Orthopedics, Shanghai Sixth People's Hospital, Shanghai Jiao Tong University, Shanghai 200233, China

[§]State Key Laboratory of High Performance Ceramics and Superfine Microstructure, Shanghai Institute of Ceramics, Chinese Academy of Sciences, Shanghai 200050, China

ABSTRACT: Prevention of implant loosening and infection is crucial to orthopedic and dental surgeries. In this work, the surface of stainless steel (SS) was modified by silver-sourced plasma immersion ion implantation (Ag-PIII). Metallic silver nanoparticles with various diameters and distributions were fabricated on the SS surfaces after treatment with Ag-PIII for 0.5 and 1.5 h, respectively. The osteogenic activity and antimicrobial properties of SS before and after Ag-PIII treatment were evaluated using in vitro and in vivo tests. The results demonstrated that Ag-PIII treatment not only promoted the antibacterial activity of SS but also enhanced the osteogenic differentiation of human bone marrow stromal cells.

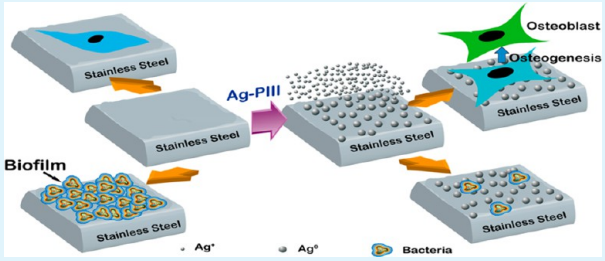

KEYWORDS: *silver, stainless steel, antimicrobial, osteogenic, plasma immersion ion implantation*

1. INTRODUCTION

Stainless steel (SS) was a standard material used in orthopedic and dental implants for its unique features in mechanics, corrosion, and cost.[1−3] Nevertheless, failures of these devices resulted by loosening and implant-associated infections.[4−6] Loosening related to the poor osseointegration of the implant materials and implant-associated infections mainly attributed to the formation of a bacterial biofilm on the implant surfaces,[7,8] in which the microbes become resistant to antibiotic therapies and the immune system of the host.[9,10] Therefore, engineering SS of both osteogenic activity and antibacterial ability is urgently needed.

Silver (Ag) had powerful activity against a broad spectrum of bacteria, including antibiotic-resistant strains, and it was extensively studied for improving the antibacterial ability of implants.[11−13] Silver nanoparticles (Ag NPs) were believed to be more reactive than the bulk metallic counterpart.[13,14] However, they, by entering mammalian cells and adversely altering the intracellular functions, were toxic at a high dosage,[15−18] which limited their applications in clinical environments. Hence, restricting the mobility of Ag NPs is a promising pathway to improve their compatibility.[10,19,20] Previous work demonstrated that Ag NPs embedded on titanium were toxic to bacterial cells but compatible to the osteoblast-like cell line MG63[20] and primary osteoblasts.[21] Apart from good cytocompatibility, it was found that Ag NPs promoted the osteogenic differentiation of stem cells at an appropriate concentration in a mobile[15] or an immobilized state.[6]

In this work, Ag NPs were immobilized on SS via silver-sourced plasma immersion ion implantation, their osteogenic activity was assessed by using human bone marrow stromal cells (hBMSCs), and their antibacterial ability was investigated with four different bacteria, including *Escherichia coli* (Gram-negative), *Pseudomonas aeruginosa* (Gram-negative), *Staphylococcus aureus* (Gram-positive), and *Staphylococcus epidermidis* (Gram-positive), and an animal model involving an implant-related femur infection in rats was also adopted.

2. MATERIALS AND METHODS

2.1. Sample Preparation and Characterization. *2.1.1. Silver-Sourced Plasma Immersion Ion Implantation (Ag-PIII).* Medical-grade 316LVM stainless steel (SS; ASTM F138, Puwei, Shanghai, China) with a nominal composition of 17.4 wt % Cr, 14.2 wt % Ni, 0.02 wt % C, 2.7 wt % Mo, 0.49 wt % Si, 1.68 wt % Mn, 0.018 wt % P, and balance Fe, was cut into various sizes, including squares (10 × 10 mm and 20 × 20 mm) for in vitro experiments, rectangles (10 × 20 mm) for ζ potential measurements, and rods (10 mm length and 1.2 mm diameter) for in vivo assessments. The SS samples were treated by Ag-PIII with a filtered cathodic arc source.[20] Silver (Ag) was doped onto the surface of SS samples for 0.5 and 1.5 h (abbreviated as 0.5h−Ag-PIII SS and 1.5h−Ag-PIII SS). The instrumental parameters are listed in Table 1.

2.1.2. Surface Structure and Chemistry. The surface morphology was observed using field-emission scanning electron microscopy (FE-SEM; S-4800, Hitachi, Tokyo, Japan), and the surface composition and chemical states were assessed by X-ray photoelectron spectroscopy (XPS; PHI 5802, Physical Electronics Inc., Eden Prairie, MN).

2.1.3. Ag Release. The Ag-PIII-treated SS samples were statically soaked in a phosphate-buffered saline solution (PBS; 10 mL) at 37 °C

Received: February 10, 2015
Accepted: May 8, 2015
Published: May 8, 2015

DOI: 10.1021/acsami.5b01310
ACS Appl. Mater. Interfaces 2015, 7, 10785−10794

Table 1. Important Ag-PIII Parameters

	target	cathodic arc
voltage pulse duration (μs)	500	500
pulsing frequency (Hz)	5	5
ion implantation voltage (kV)	−30	
pressure (Pa)	5×10^{-3}	

for 30 days. The amounts of Ag released into the solutions were determined by analyzing the solutions by inductively coupled plasma optical emission spectrometry (Nu Instruments, Wrexham, U.K.).

2.1.4. Surface ζ Potentials. The ζ potentials of the samples were assessed using a Surpass electrokinetic analyzer (Anton Parr, Graz, Austria). A solution of 0.9% sodium chloride was used as the testing medium. The pH values of the solution were changed by adding HCl or NaOH.[6]

2.1.5. Water Contact Angles. The water contact angles of the samples were measured on a contact-angle instrument (SL200B; Shanghai Solon Information Technology Co., Ltd., Shanghai, China).[22]

2.2. Evaluation of the in Vitro Cytocompatibility. *2.2.1. Cell Culture of Mesenchymal Stem Cells (MSCs).* hBMSCs (Stem Cell Bank, Chinese Academy of Sciences, Shanghai, China) were cultured in a regular growth medium consisting of an α-minimum essential medium (α-MEM; Gibco Invitrogen, Inc., Carlsbad, CA) supplemented with 10% fetal bovine serum (HyClone, South Logan, UT), 0.3 mg/mL glutamine (HyClone), 100 U/mL penicillin, and 100 μg/mL streptomycin at 37 °C in a humidified atmosphere of 5% CO_2. The cells of passage 3−5 were used in the experiments. The 10 and 20 mm square samples were placed in 24- and 6-well plates (Costar), respectively, and the hBMSCs were seeded at different densities for the following assays.

2.2.2. Cytocompatibility Evaluation. To assess the cytotoxicity, the cells were seeded at a density of 2×10^4 cells/well. After 3 days, the culture medium was collected and centrifuged, and the lactate dehydrogenase (LDH) activity, a mark of toxicity, in the supernatant was detected based on the instructions of the manufacturer (Beyotime Institute of Biotechnology, Shanghai, China).

To assess the adhesion and spreading behaviors, the cells were seeded at a density of 4×10^4 cells/well, incubated for 1, 4, and 24 h, then rinsed with PBS, fixed with a 4% formaldehyde solution, permeabilized with 0.1% (v/v) Triton X-100 (Amresco, Solon, OH), and stained with rhodamine phalloidin (Invitrogen) and 4′,6-diamidino-2-phenylindole (DAPI; Sigma, St. Louis, MO). The cytoskeletal actin and cell nuclei were examined by confocal laser scanning microscopy (CLSM; LSM 510 Meta, Zeiss, Oberkochen, Germany).

To observe the cell morphology on samples, the cells were seeded at a density of 1×10^4 cells/well and cultured for 1, 3, and 7 days. At each time point, the cells on the samples were observed by a scanning electron microscopy (SEM; JSM-6310LV, JEOL, Tokyo, Japan) with the method described in our previous report.[10]

To assess the cell proliferation and viability, the cells were seeded at a density of 1×10^4 cells/well and cultured for 1, 3, and 7 days. At each time point, the cell viability was determined by the Cell Counting Kit-8 assay (CCK-8; Beyotime).

2.2.3. Alkaline Phosphatase (ALP) Assay. The cells were seeded at a density of 2×10^4 cells/well and cultured in a growth medium or in an osteogenic differentiation medium (α-MEM supplemented with ascorbic acid, glycerophosphate, and dexamethasone). The ALP activity at days 7 and 14 was measured by an alkaline phosphatase kit (Beyotime) according to the manufacturer's instructions. Values were normalized against the protein concentration, which was determined by a BCA protein assay kit (Pierce Biotechnology, Rockford, IL).

2.2.4. Extracellular Matrix (ECM) Mineralization Assay. The cells were seeded at a density of 2×10^4 cells/well and cultured in a growth medium or in an osteogenic differentiation medium for 21 days. After washing with PBS and fixation with a 4% formaldehyde solution, Alizarin Red (40 mM pH 4.2; Beijing Solarbio Science & Technology Co., Ltd., Beijing, China) was used to evaluate ECM mineralization. To quantify the matrix mineralization, the stain was dissolved in 10% cetylpyridinum chloride in 10 mM sodium phosphate (pH 7). The absorbance of the released Alizarin Red S was measured at 620 nm.

2.2.5. Quantitative Real-Time Polymerase Chain Reaction (qRT-PCR) Assay. The cells were seeded at a density of 1×10^5 cells/well in a growth medium or an osteogenic differentiation medium. After 14 days, the total RNA was isolated using Trizol reagent (Invitrogen). A total of 1 μg of RNA was then reverse-transcribed into complementary DNA using a PrimeScript RT reagent kit (Takara Bio Inc., Shiga, Japan). Expressions of the osteogenesis-related genes including ALP, bone morphogenic protein-2 (BMP-2), runt-related transcription factor 2 (Runx2), and osteocalcin (OCN) were analyzed on the Bio-Rad C1000 using SYBR Premix Ex Taq II (Takara). The housekeeping gene GAPDH was used to normalize the relative expressions of the above genes. The primers used are listed in Table 2.

2.2.6. Western Blot Assay. To investigate the activity of the extracellular signal-related kinases (ERK)1/2 signaling of the cells on the samples, the cells were seeded at a density of 1×10^5 cells/well. After being cultured for 24 h, the cells were washed in ice-cold PBS and solubilized in an ice-cold lysis buffer [50 mM Tris HCl, 0.5 mM ethylenediaminetetraacetic acid (EDTA), 50 mM sodium fluoride, 0.1% sodium dodecyl sulfate, 1% Nonidet P-40, 50 mM β-glycerophosphate, and proteinase inhibitors]. ERK1/2 and pERK1/2 were measured using the method mentioned in the literature.[23]

2.3. Antibacterial Assay. *2.3.1. Bacteria Preparation and Characterization.* Freeze-dried *E. coli* (ATCC 25922), *P. aeruginosa* (ATCC 27853), *S. aureus* (ATCC 43300), and *S. epidermidis* (ATCC 35984) were obtained from the American Type Culture Collection (Rockefeller, MD). According to the method used in our previous study,[24] the above three strains were prepared at a concentration of 1×10^6 colony forming units (CFUs)/mL in Trypticase Soy Broth (TSB; BD Biosciences, Franklin Lakes, NJ) for in vitro experiments, and *S. aureus* was prepared at a concentration of 1×10^5 CFUs/mL in PBS for in vivo experiments.

2.3.2. In Vitro Antibacterial Assay. The antibacterial effect of the samples was analyzed by a spread plate method (SPM), CLSM, and SEM. A total of 100 μL of a bacterial suspension (1×10^6 CFUs/mL) was added to each of the samples in a 24-well plate and statically incubated at 37 °C for 24 h. Then, the samples were mildly washed with PBS three times. The following procedures were detailed in our previous report.[10]

2.3.3. In Vivo Antibacterial Assessment. The experimental protocol was approved by the Animal Care and Experiment Committee of Shanghai Sixth People's Hospital affiliated with Shanghai Jiao Tong University, School of Medicine. Eight male, 3-month-old Sprague−Dawley rats with an average weight of 220 g (160−280 g) were used. After intraperitoneal injection of 4% chloral

Table 2. Primers Used in This Study

gene	forward primer sequence (5-3)	reverse primer sequence (5-3)
Runx2	CCAACCCACGAATGCACTATC	TAGTGAGTGGTGGCGGACATAC
OCN	CGCTACCTGTATCAATGGCTGG	CTCCTGAAAGCCGATGTGGTCA
BMP-2	GAGAAGGAGGAGGCAAAGAAA	AGCAGCAACGCTAGAAGACAG
ALP	AACGTGGCCAAGAACATCATCA	TGTCCATCTCCAGCCGTGTC
GAPDH	ATCCCATCACCATCTTCC	GAGTCCTTCCACGATACCA

DOI: 10.1021/acsami.5b01310
ACS Appl. Mater. Interfaces 2015, 7, 10785−10794

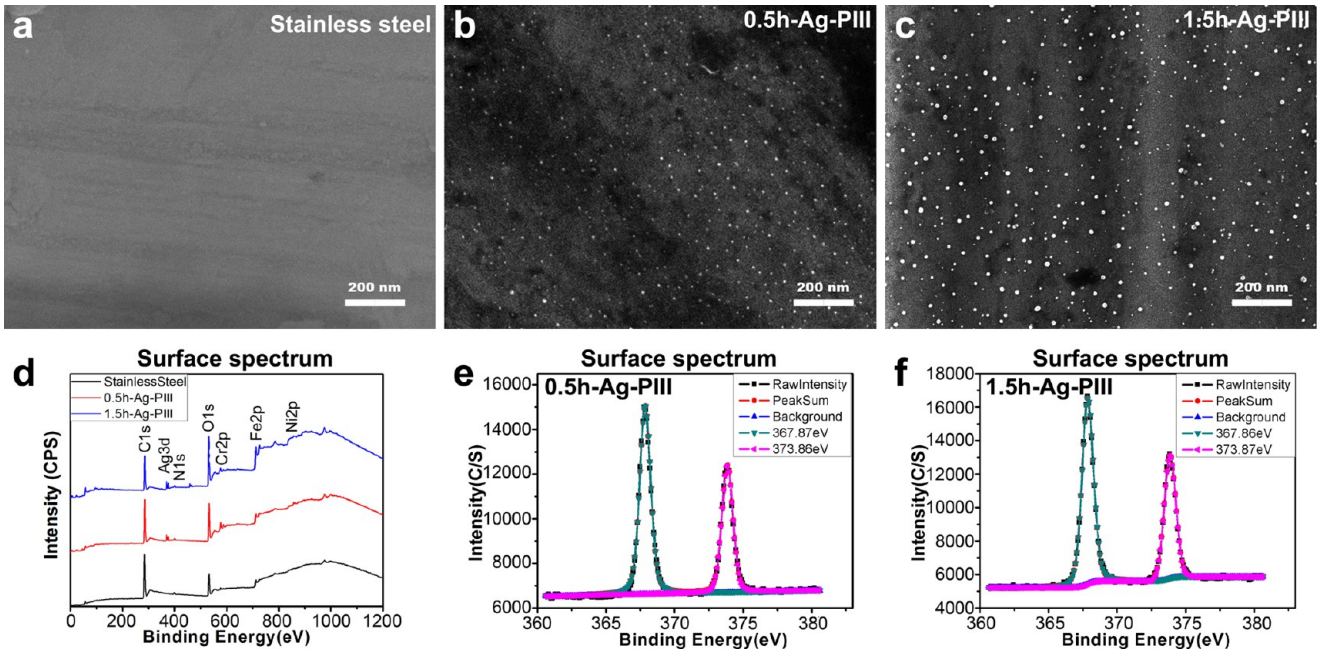

Figure 1. Surface views of SS before and after Ag-PIII treatment: (a) SS, (b) 0.5h−Ag-PIII SS and (c) 1.5h−Ag-PIII SS. XPS full spectra of samples (d) and XPS Ag 3d spectra of the Ag-PIII SS surface: (e) 0.5h−Ag-PIII SS; (f) 1.5h−Ag-PIII SS.

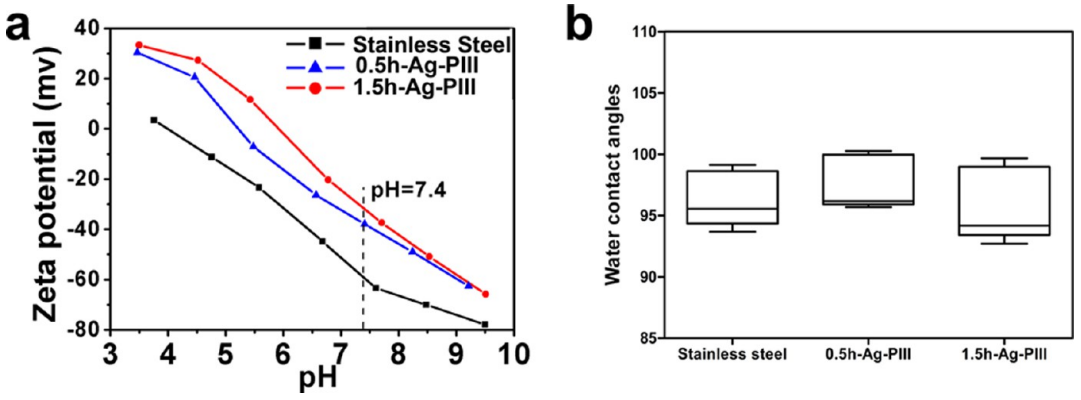

Figure 2. ζ potentials versus pH (a) and water contact angles (b) acquired from SS before and after Ag-PIII treatment.

hydrate (0.9 mL/100 g body weight), a 30 mm longitudinal left femoral anterolateral incision was made. Then the femoral shaft was exposed, and three canals perpendicular to the femur with 8 mm spacing were drilled using a Kirschner wire (1.2 mm diameter). After SS wire was inserted into the distal canal, 1.5h−Ag-PIII wire to the middle one and 0.5h−Ag-PIII wire to the proximal one, the overlying muscle and fascia were closed. Then, the femoral medullary cavity was opened, and 50 μL of a prepared *S. aureus* suspension was injected into it using the method mentioned in our previous study.[24]

2.3.3.1. Radiograph and Microcomputed Tomography Scanning. At 0, 2, 4, and 6 weeks postsurgery, lateral radiographs of the femur were obtained. Three independent observers with no prior knowledge of the study group evaluated the radiographs, focusing on periosteal reaction, osteolysis, and general impression according to the literature.[25] At 6 weeks postsurgery, the animals were euthanized, and the operated femurs were harvested, fixed in 10% neutral buffered formalin for 72 h, and then scanned by a microcomputed tomography (microCT; 1172, Skyscan Microtomography, Kontich, Belgium) at an image resolution of 18 μm (55 kVp and 181 mA radiation source with a 0.5 mm aluminum filter).

2.3.3.2. Histopathological Evaluation. After microCT scanning, the femurs were decalcified in a 10% EDTA solution (pH 7.4) for 14 days and then washed, dehydrated, and embedded in paraffin. Then 5 mm sagittal sections of each specimen were cut, and hematoxylin and eosin (H&E) and Giemsa staining were used to assess the morphology and bacterial contamination, respectively.

2.4. Statistical Analysis. Statistically significant differences (p) were analyzed by one-way ANOVA and Student−Newman−Keuls post hoc tests using *SPSS 18* software, and $p < 0.05$ were considered to be significant.

3. RESULTS

3.1. Material Characterization. The surface microstructures of the SS samples before and after Ag-PIII treatment were observed by SEM. Compared to the original SS (Figure 1a), homogeneously distributed spherical particles were detected on both Ag-PIII samples. For 0.5h−Ag-PIII (Figure 1b), the particle diameter was about 7 nm and there were about 2.78×10^8 particles/ mm^2. As the Ag-PIII duration was increased to 1.5 h (Figure 1c), the particle became larger and the distributions in diameter became bimodal, with one peak at about 5 nm and the other at about 16 nm. The particle density increased to 4.17×10^8. The result indicated that the amount and size of Ag NPs was highly related to the duration of PIII. The samples were further analyzed by XPS, and the results revealed that the original SS contained Fe, Cr, and Ni but no

DOI: 10.1021/acsami.5b01310
ACS Appl. Mater. Interfaces 2015, 7, 10785−10794

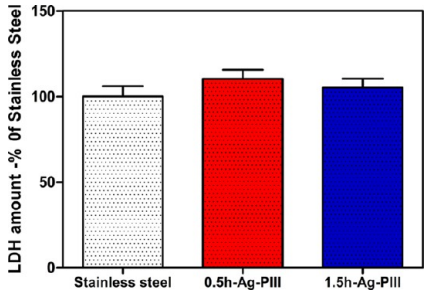

Figure 3. Amounts of LDH released by hBMSCs to the culture medium in the first 3 days of incubation.

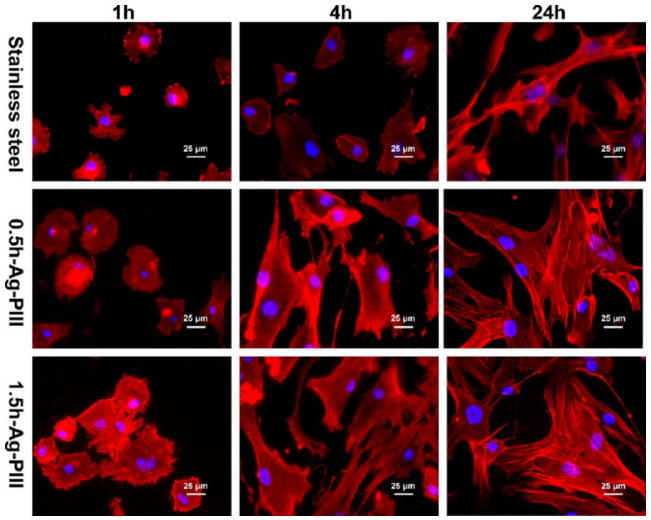

Figure 4. Fluorescent images of hBMSCs cultured on various surfaces for 1, 4, and 24 h with actin stained using rhodamine phalloidin (red) and nuclei stained using DAPI (blue).

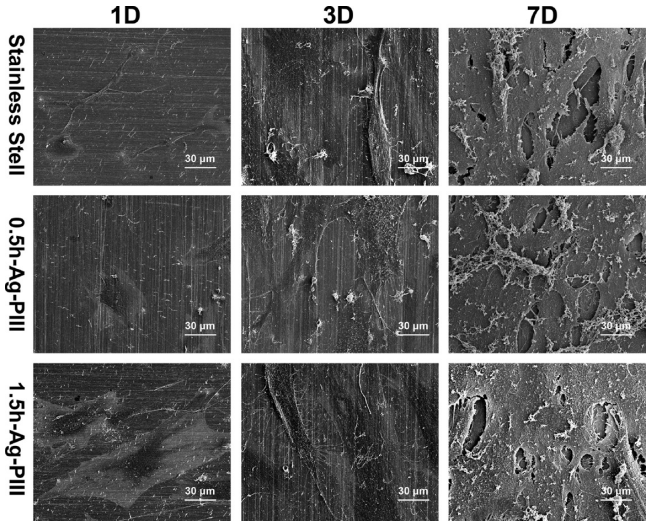

Figure 5. SEM morphology of hBMSCs cultured on various surfaces for 1, 3, and 7 days.

Ag (Figure 1d). However, Ag was evidenced on the Ag-PIII samples. As shown in Figure 1e,f, the Ag 3d doublet at about 374.02 eV (Ag $3d_{3/2}$) and 368 eV (Ag $3d_{5/2}$) indicates that the Ag-PIII surface contains metallic Ag. The amounts of Ag released from the Ag-PIII SSs were detected by immersing them in PBS and incubating at 37 °C for 1 month. There was no Ag detected in PBS.

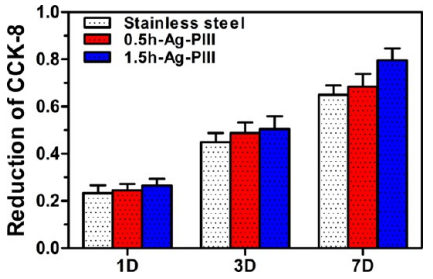

Figure 6. CCK-8 viability of hBMSCs cultured on various surfaces for 1, 3, and 7 days.

Because the surface charge is important to cell adhesion,[26] the surface ζ potentials of the samples were detected. Figure 2a depicted the ζ potential versus pH plots of the samples. The ζ potentials at pH 7.4 of both Ag-PIII samples were more positive than that of SS, and 1.5h−Ag-PIII had the most positive ζ potential. In addition, the water contact angles for 0.5h−Ag-PIII and 1.5h−Ag-PIII were 97.59 ± 2.19° and 95.79 ± 3.01°, respectively, which were comparable to that of SS, 96.3 ± 2.26°, suggesting that Ag-PIII treatment did not change the surface wettability of SS (Figure 2b).

3.2. Response of hBMSCs. The release of LDH was measured to assess the cytocompatibility of the samples. As the results show in Figure 3, the LDH concentrations are comparable among the three sample groups, indicating that no obvious cytotoxicity was introduced to SS by Ag-PIII treatment.

The initial adhesion and spreading behavior of hBMSCs were assessed by staining with rhodamine phalloidin and DAPI. As the results show in Figure 4, most of the cells on SS exhibit a spherical morphology in the first 1 h while cells on the Ag-PIII samples spread well. After being cultured 24 h, polygonal cells with strong expressions of F-actin, filopodia, and lamellipodia were common to Ag-PIII samples, especially 1.5h−Ag-PIII, whereas the cells on SS were usually spindle-shaped and lacked expressions of F-actin and filopodia extensions. The results indicated that the initial adhesion and spreading activity of hBMSCs could be best improved by the Ag-PIII and 1.5h−Ag-PIII groups.

The cell morphology on the samples at days 1, 3 and 7 was observed by SEM (Figure 5). At day 1, the cells on SS showed a slender shape, while those on Ag-PIII were extended, exhibiting a typical polygonal shape, especially on 1.5h−Ag-PIII, which was consistent with the results obtained by fluorescent assay (Figure 4). However, when the culture time exceeded 3 days, the difference in the cell morphology became unremarkable, the hBMSCs on the three samples were all spread well with a large number of filopodia, and the cells completely covered the material surfaces at day 7.

The proliferation and vitality of hBMSCs were evaluated by CCK-8 assay. As the results presented in Figure 6 show, although no statistically difference in the cell proliferation of the samples was detected, a trend of 1.5h−Ag-PIII SS > 0.5h−Ag-PIII SS > SS was sketched out, and it became more obvious at day 7, indicating that Ag-PIII was favorable to cell proliferation, with the best activity from 1.5h−Ag-PIII.

The osteogenic differentiation of hBMCs was further assessed by ALP, ECM mineralization, and qRT-PCR assays. Compared to SS, whether in an osteogenic medium or a growth

DOI: 10.1021/acsami.5b01310
ACS Appl. Mater. Interfaces 2015, 7, 10785−10794

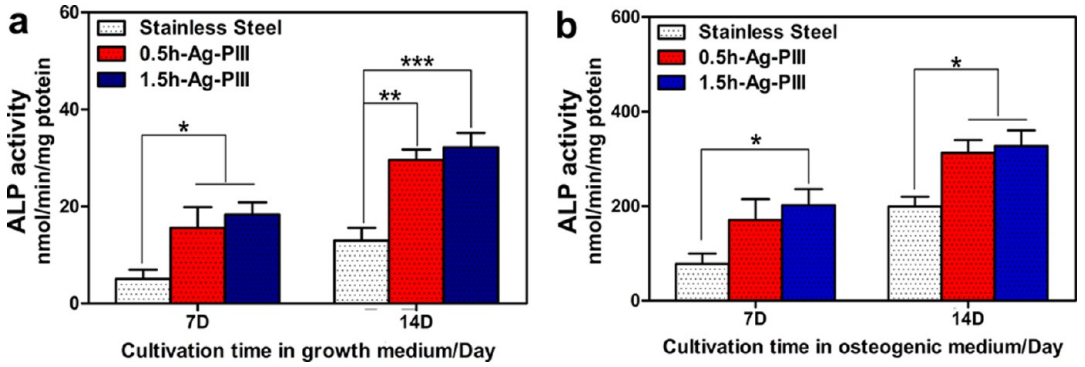

Figure 7. ALP activity of hBMSCs cultured on various surfaces in a growth medium (a) and an osteogenic differentiation medium (b) for 7 and 14 days: (*) $P < 0.05$; (**)$P < 0.01$; (***) $P < 0.001$.

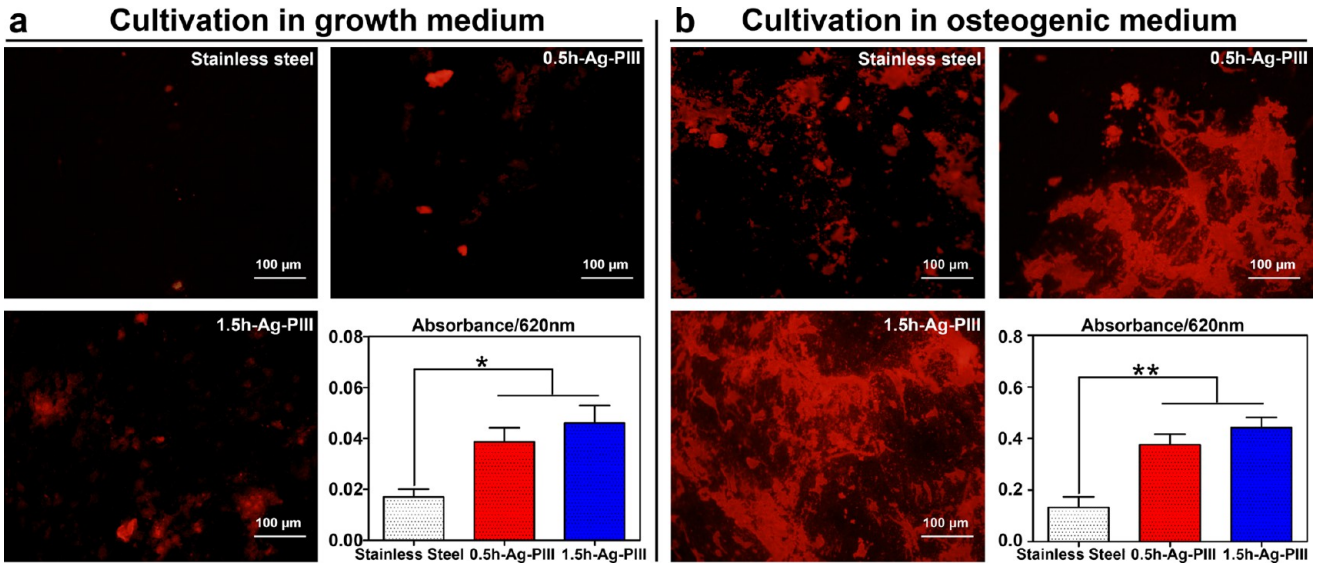

Figure 8. Matrix mineralization of hBMSCs cultured on various surfaces in a growth medium (a) and an osteogenic differentiation medium (b) for 21 days: (*) $P < 0.05$; (**) $P < 0.01$.

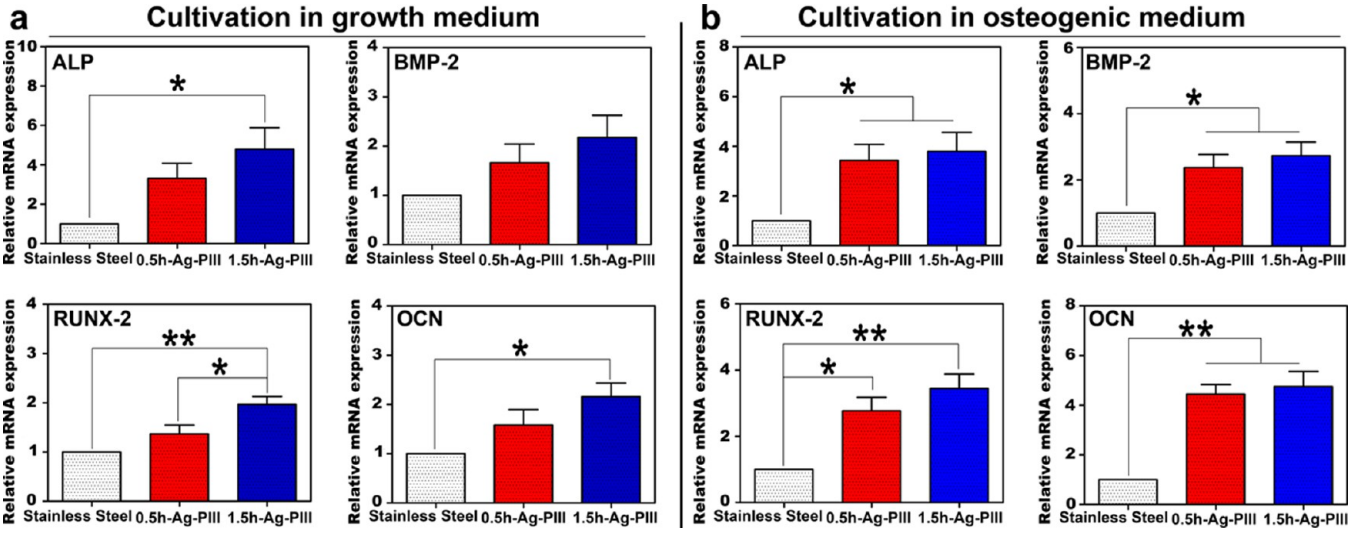

Figure 9. qRT-PCR analysis: ALP, BMP-2, Runx2, and OCN expressions by hBMSCs on various surfaces in a growth medium (a) and an osteogenic differentiation medium (b) after incubation for 14 days: (*) $P < 0.05$; (**) $P < 0.01$.

medium, Ag-PIII samples obviously improved the ALP activity of the cell at days 7 and 14 (Figure 7), enhanced the level of ECM mineralization at day 21 (Figure 8), and promoted the gene expressions of ALP, BMP-2, Runx2, and OCN at day 14 (Figure 9), and 1.5h−Ag-PIII SS was the best. The results indicate that Ag-PIII treatment promoted the osteogenic

DOI: 10.1021/acsami.5b01310
ACS Appl. Mater. Interfaces 2015, 7, 10785−10794

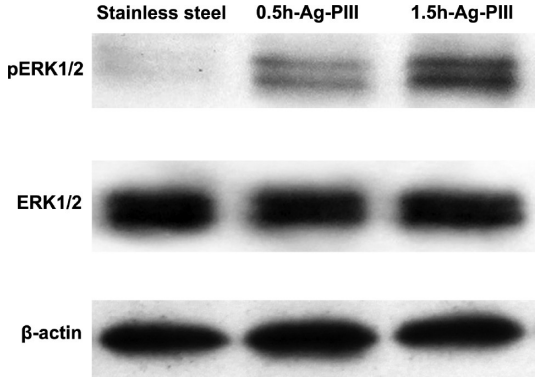

Figure 10. Western blots of the pERK1/2 and ERK1/2 levels in hBMSCs cultured on various surfaces for 24 h.

differentiation of hBMSCs, especially 1.5h−Ag-PIII. Moreover, Western blot assay was used to evaluate the activity of the ERK1/2 signaling, and the results demonstrate (Figure 10) that the pERK1/2 protein level, representing the ERK activation status, was significantly improved by Ag-PIII, especially 1.5h−Ag-PIII.

3.3. In Vitro Antibacterial Property. The antibacterial rate (Ra) was quantitatively evaluated by a SPM. As shown in Figure 11, the Ra values of 0.5h−Ag-PIII and 1.5h−Ag-PIII reached 78.9% and 91.4% for *E. coli*, 78.3% and 89.7% for *P. aeruginosa*, 76.7% and 84.3% for *S. epidermidis*, and 80% and 83.7% for *S. aureus*, respectively, indicating that Ag-PIII inhibited bacterial proliferation regardless of the species. Moreover, the antibacterial rates did not obviously deteriorate even after seven cycles of bacterial exposure, suggesting that the Ag-PIII samples had stable antibacterial activity.

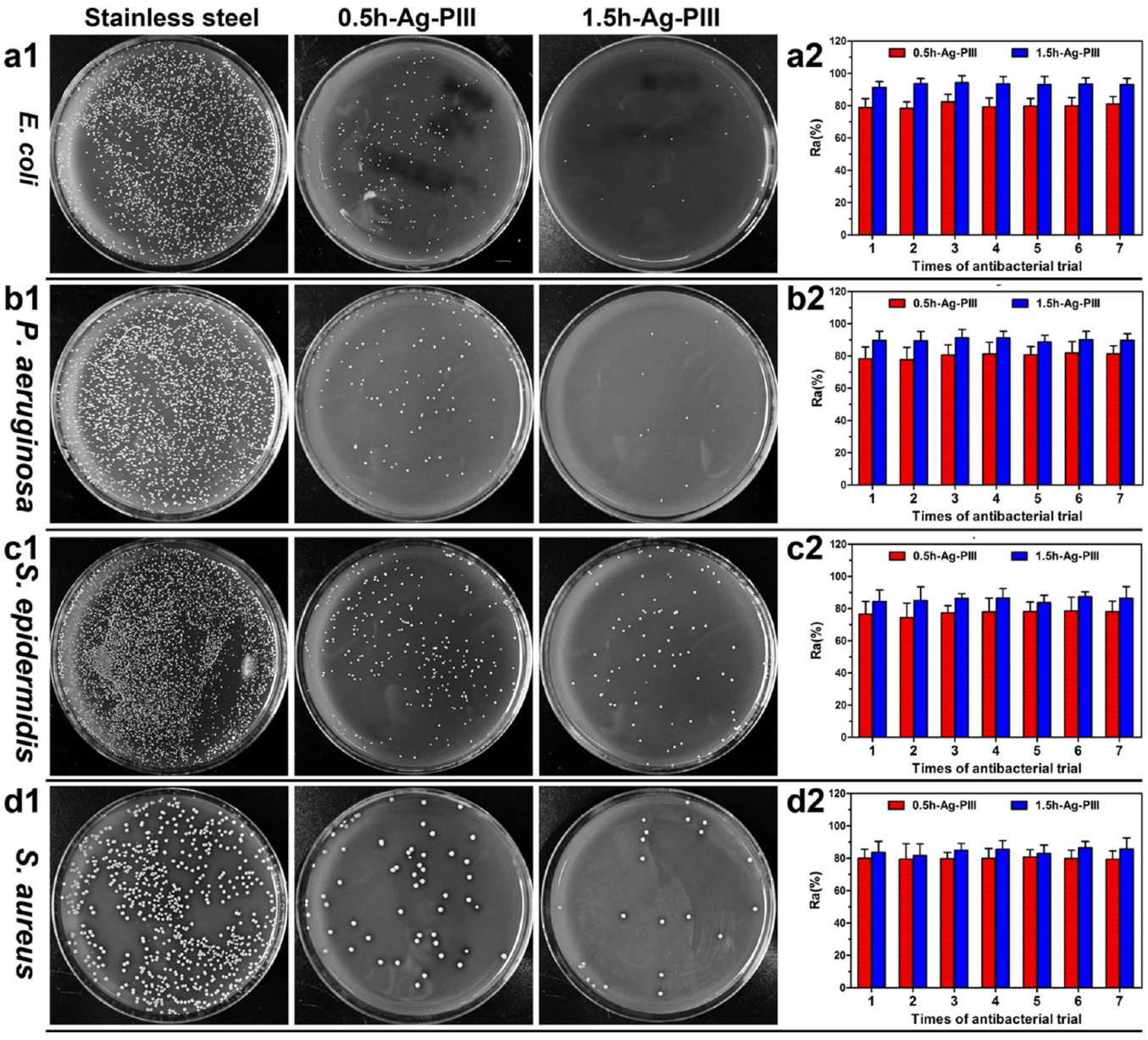

Figure 11. Recultivated bacterial colonies on agar after bacteria dissociation from the various surfaces and antibacterial rates (Ra) was used to estimate the amount of living bacteria on Ag-PIII SS: (a1) 2 for *E. coli*; (b1) 2 for *P. aeruginosa*; (c1) 2 for *S. epidermidis*; (d1) 2 for *S. aureus*.

DOI: 10.1021/acsami.5b01310
ACS Appl. Mater. Interfaces 2015, 7, 10785−10794

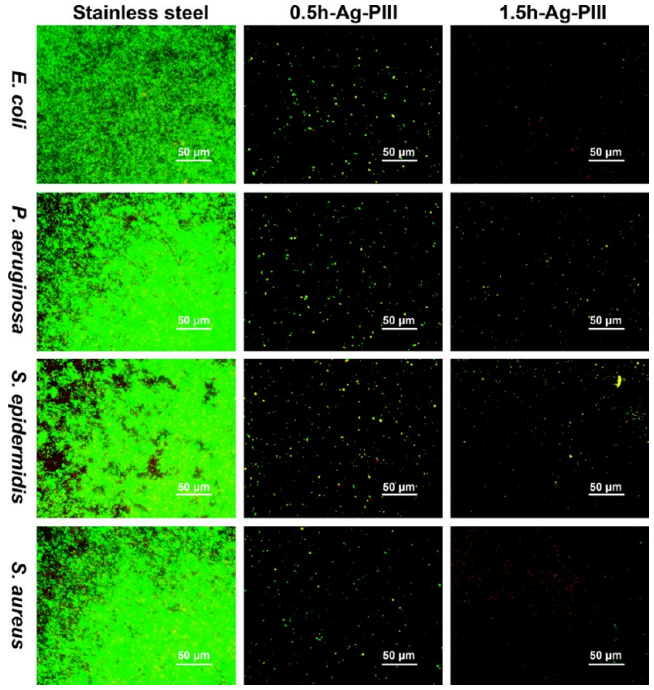

Figure 12. Fluorescent images of bacteria on various surfaces after staining with the Baclight dead/live stain after incubation for 24 h.

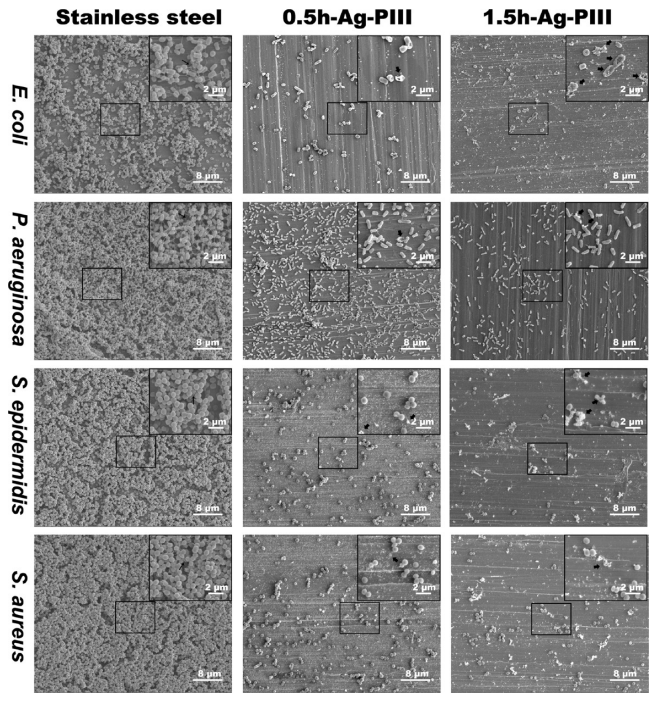

Figure 13. SEM morphology of bacteria on various surfaces after incubation for 24 h. Thin and thick arrows mark the filamentous structure among bacteria in a biofilm and the ruptured, lysed cell, respectively.

The antibacterial ability of Ag-PIII was also verified by CLSM and SEM. The CLSM views (Figure 12) showed that an intense green fluorescence on the surface of SS was observed after culturing for 24 h, which indicated that the material was good for bacterial adhesion and formation of a biofilm, and a sparsely distributed and less green fluorescence and more red fluorescence were found on the surfaces of Ag-PIII,

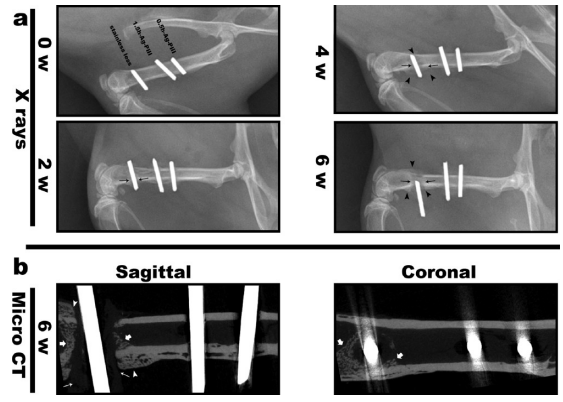

Figure 14. Radiographical images: (a) X-ray images of the left femur in lateral view implanted with the three kinds of wire implants at 0, 2, 4, and 6 weeks postsurgery. Radiographical signs of osteolysis (black thin arrow) and periosteal new bone formation (black arrowhead) surrounding the SS wires are observed at 2 weeks and aggravate with time. At 6 weeks postsurgery, the SS wire is found to loosen and shift. No signs of osseous infection are observed around the Ag-PIII SS wires, and no loosening can be found. (b) 2D microCT images of the left femur at 6 weeks postsurgery. Bone resorption (white thin arrow) around the SS wire and new generated bone (white thick arrow) blocking the medullary cavity are detected. No such findings around the Ag-PIII SS wire can be observed. (The loose SS wire was dropped out when the femur was harvested and then put back into the original canal before microCT examination.)

demonstrating better activity against bacterial adhesion and formation of a biofilm. SEM observations (Figure 13) revealed a similar trend, which displayed that the bacteria on SS were conglomerated into grapelike colonies through a filopodia-like structure, indicating the synthesis of glycocalyx and formation of a biofilm.[9,10] In contrast, not many bacteria were found on Ag-PIII, and some of them displayed abnormal morphology, such as distorted and broken shape, suggesting that bacteria adhesion, viability, and biofilm formation on Ag-PIII were inhibited. Amoung the Ag-PIII groups, 1.5h−Ag-PIII had the least amount of bacteria cells and the highest antibacterial rate, which was consistent with the results obtained by a SPM and CLSM.

3.4. In Vivo Antibacterial Property. *3.4.1. Radiographical Assessment.* As shown in Figure 14a, obvious radiographic signs of osseous destruction and periosteal reaction were detected around the SS wire. In contrast, no osteolysis and periosteal reaction were detected around the Ag-PIII wires. These results were confirmed by microCT (Figure 14b), which showed that the SS wire was loosened, indicating that a serious infection occurred around the sample. Moreover, a large amount of new bone formed away from the SS wire and blocked the medullary cavity, indicating the occurrence of chronic osteomyelitis. In contrast, no infectious osteogenesis was found in the medullary cavity, but a small amount of new bone was formed surrounding the Ag-PIII samples.

3.4.2. Histological Evaluation. The histological slices of H&E staining (Figure 15) show typical signs of bone infection, as manifested by the development of abscess lesions, destruction of cortical bone, periosteal new bone formation, and closure of the medullary cavity. A large number of fibrous tissues without bone formation were observed around the SS wire. Giemsa staining slices reveal that there were lots of bacteria at the interface between the SS wire and fibrous tissue and in the intramedullary tissues. In comparison, there was no

DOI: 10.1021/acsami.5b01310
ACS Appl. Mater. Interfaces 2015, 7, 10785−10794

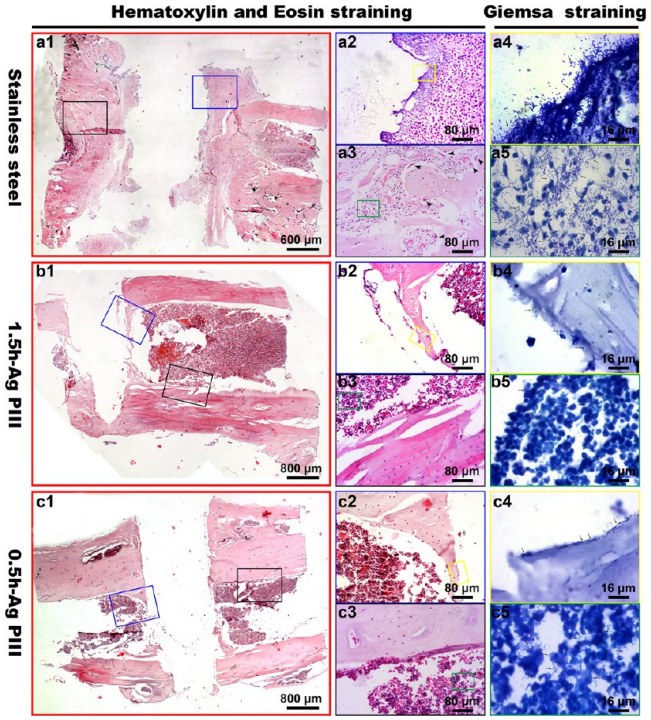

Figure 15. Histological slices in sagittal plane images perpendicular to implants stained with H&E and Giemsa staining at 6 weeks postsurgery. An overview image (a1) reveals a large number of fibrous tissues but no bone formation around the SS wire, destruction of cortical bone, periosteal new bone formation, and closure of the medullary cavity. Close-up views (a2–a5) show fibrous tissue formation around the SS wire (a2), osteoclasts (arrowheads) invasion bone (a3), and lots of bacteria (arrows) persistence in the fibrous tissue around the SS wire (a4) and the intramedullary tissue (a5). Overview images (b1 and c1) display direct new bone formation surrounding the Ag-PIII SS wire and no obvious bone destruction and periosteal new bone formation. Close-up views (b2–b5 and c2–c5) show bone formation at the interface of the Ag-PIII SS wire (b2 and c2), no osteoclasts invasion bone (b3 and c3), and a very small amount of bacteria contamination on the bone around the Ag-PIII SS wire (b4 and c4) and in the intramedullary tissue (b5 and c5). An arrowhead and an arrow mark the osteoclast and bacteria, respectively.

obvious bone destruction and periosteal new bone formation but direct new bone formation surrounding the two Ag-PIII samples. Moreover, only a few bacteria existed around the Ag-PIII samples, and the amount of bacteria in the intramedullary tissues around Ag-PIII was also much less than that around the SS wire. These results indicate that the Ag-PIII samples exhibited excellent antibacterial activity and were able to stimulate healthy bone formation in vivo.

4. DISCUSSION

Taking together, implant infection and loosening are two main reasons for the failure of fixation,[27] so the design of new implant materials possessing both osteogenic and antibacterial ability is needed. In this study, Ag NPs were fabricated and in situ immobilized on SS by Ag-PIII. In vitro and in vivo results demonstrated that Ag-PIII treatment not only promoted the antibacterial activity of SS but also enhanced the adhesion, spreading, proliferation, and osteogenic differentiation of hBMSCs.

The Ag NPs produced by Ag-PIII were immobile and releasea a negligible amount of Ag ions; hence, the Ag-PIII samples had no obvious cytotoxicity according to LDH assay (Figure 3). Moreover, Ag-PIII treatment dramatically promoted cell spreading at the early stage (24 h; Figures 4 and 5). This trend can be attributed to the relatively more positive ζ potentials of the samples (Figure 2a), which was beneficial to the initial adhesion of mammalian cells.[6] It is believed that well-spread hBMSCs with enhanced expression of F-actin are good for osteogenic differentiation.[23,28,29] In this study, the improved osteogenic differentiation property for Ag-PIII samples was confirmed by ALP, ECM mineralization, and qRT-PCR assays. The ERK1/2 signaling was believed to play a critical role in the osteogenic differentiation of MSCs.[30−32] The pERK1/2 protein level of the hBMSCs was significantly promoted after their adhesion to the Ag-PIII samples, which is consistent with the report that good cell spreading on biomaterials initiates the ERK1/2 signaling.[23] These results demonstrate that the immobilized Ag NPs rendered SS of good compatibility, which improved the spreading of hBMSC, initiated the ERK1/2 signaling, up-regulated the osteogenesis-related gene expressions, and eventually promoted osteogenic differentiation. Also, these effects were proportional to the duration of the Ag-PIII treatment, which determined the amount and size of the Ag NPs.

In addition to improving the biocompatibility of SS, the main purpose of Ag-PIII was to provide SS with antibacterial properties. In order to test the antibacterial activity of the Ag-PIII samples, four different kinds of bacteria were evaluated by three distinct techniques in vitro. Microbiological counting, providing a quantitative estimate of the number of viable bacteria in a biofilm, and CLSM and SEM, focusing on the structure of the biofilm and the state of bacteria, except for showing the number of bacteria, consistently showed that Ag-PIII treatment was effective in inhibiting bacteria adhesion and biofilm formation, irrespective of the kind of bacteria, and the longer time for Ag-PIII, producing higher number and larger size of Ag NPs on SS, generated better antibacterial effects (the activity of 0.5h−Ag-PIII against bacteria was weaker than that of 1.5h−Ag-PIII), which is consistent with our previous research.[10] Besides, the Ag-PIII samples released minimal Ag ions and their antibacterial activity did not deteriorate after multiple cycles of bacterial exposure, indicating that the antibacterial action of the Ag-PIII SS was independent of Ag release and likely a result of the synergetic effects of Ag and the SS substrate. Also, further studies need to be done to investigate the exact antibacterial mechanism.

The antibacterial activity of the Ag-PIII samples was further assessed in vivo using an implant-related infection in rats. The Ag-PIII samples released a negligible amount of Ag ion and acted against bacteria through direct contact; therefore, the three sample groups were implanted in the same rat femur to evaluate the antibacterial activity in vivo. According to Figures 14 and 15, obvious osseous destruction, periosteal reaction, and lots of bacteria occurred around the SS wire, whereas no osseous destruction, periosteal reaction, and only a few bacteria were observed surrounding the Ag-PIII samples, which indicated that the SS wire provided a surface to foster bacterial adhesion and biofilm growth; however, bacterial adhesion and biofilm formation was inhibited on the surface of the Ag-PIII SS wires. In addition, new bone formation on the surface of the Ag-PIII SS wires and only fibrous tissue surrounding the SS wire were found, indicating that the Ag-PIII SS had good osteogenic ability. The results showed that the Ag-PIII SS could inhibit implant-related infection and, meanwhile, induce bone

DOI: 10.1021/acsami.5b01310
ACS Appl. Mater. Interfaces 2015, 7, 10785−10794

formation, which was consistent with the results obtained in vitro.

5. CONCLUSION

Ag NPs supported on SS can be fabricated by Ag-PIII. The SS-immobilized Ag NPs inhibited bacterial adhesion and biofilm formation in vitro and reduced implant-associated infection in vivo. Moreover, the Ag-PIII-treated SS exhibited no apparent cytotoxicity but promoted osteogenic differentiation of hBMSCs by improving cell spreading, initiating the ERK1/2 signaling, and up-regulating the osteogenesis-related gene expressions. The improved osteogenic and antibacterial ability were independent of Ag release. By optimization of the Ag-PIII conditions, SS can be endowed with both osteogenic and antibacterial abilities, which bode well for prolonged clinical use.

AUTHOR INFORMATION

Corresponding Authors

*E-mail: zhangxianl197826@163.com.
*E-mail: xyliu@mail.sic.ac.cn.

Author Contributions

‡These authors contributed equally.

Notes

The authors declare no competing financial interest.

ACKNOWLEDGMENTS

Financial support from the National Basic Research Program of China (973 Program; Grant 2012CB933600), National Natural Science Foundation of China (Grants 81271962, 81301571, 8111704, and 31370962), Shanghai Committee of Science and Technology, China (Grants 11DJ1400304, 12441903102, and 14XD1403900), Shanghai Rising-Star Program (Grant 15QA1404100), Youth Innovation Promotion Association CAS (Grant 2015204), and Open Research Fund of State Key Laboratory of Bioelectronics, Southeast University, the Opening Project of State Key Laboratory of High Performance Ceramics and Superfine Microstructure (Grant SKL201206SIC) is acknowledged.

REFERENCES

(1) Devasconcellos, P.; Bose, S.; Beyenal, H.; Bandyopadhyay, A.; Zirkle, L. G. Antimicrobial Particulate Silver Coatings on Stainless Steel Implants for Fracture Management. *Mater. Sci. Eng., C* **2012**, *32*, 1112−1120.

(2) Disegi, J. A.; Eschbach, L. Stainless Steel in Bone Surgery. *Injury* **2000**, *31*, 2−6.

(3) Kenar, H.; Akman, E.; Kacar, E.; Demir, A.; Park, H.; Abdul-Khaliq, H.; Aktas, C.; Karaoz, E. Femtosecond Laser Treatment of 316L Improves Its Surface Nanoroughness and Carbon Content and Promotes Osseointegration: An in vitro Evaluation. *Colloids Surf., B* **2013**, *108*, 305−312.

(4) Neoh, K. G.; Hu, X.; Zheng, D.; Kang, E. T. Balancing Osteoblast Functions and Bacterial Adhesion on Functionalized Titanium Surfaces. *Biomaterials* **2012**, *33*, 2813−2822.

(5) Zhao, L.; Chu, P. K.; Zhang, Y.; Wu, Z. Antibacterial Coatings on Titanium Implants. *J. Biomed. Mater. Res., Part B* **2009**, *91*, 470−480.

(6) Jin, G.; Qin, H.; Cao, H.; Qian, S.; Zhao, Y.; Peng, X.; Zhang, X.; Liu, X.; Chu, P. K. Synergistic Effects of Dual Zn/Ag Ion Implantation in Osteogenic Activity and Antibacterial Ability of Titanium. *Biomaterials* **2014**, *35*, 7699−7713.

(7) Gristina, A. G.; Costerton, J. W. Bacterial Adherence to Biomaterials and Tissue. The Significance of Its Role in Clinical Sepsis. *J. Bone Jt. Surg., Am. Vol.* **1985**, *67*, 264−273.

(8) Gristina, A. G.; Oga, M.; Webb, L. X.; Hobgood, C. D. Adherent Bacterial Colonization in the Pathogenesis of Osteomyelitis. *Science* **1985**, *228*, 990−993.

(9) Antoci, V., Jr.; Adams, C. S.; Parvizi, J.; Davidson, H. M.; Composto, R. J.; Freeman, T. A.; Wickstrom, E.; Ducheyne, P.; Jungkind, D.; Shapiro, I. M.; Hickok, N. J. The Inhibition of Staphylococcus Epidermidis Biofilm Formation by Vancomycin-modified Titanium Alloy and Implications for the Treatment of Periprosthetic Infection. *Biomaterials* **2008**, *29*, 4684−4690.

(10) Qin, H.; Cao, H.; Zhao, Y.; Zhu, C.; Cheng, T.; Wang, Q.; Peng, X.; Cheng, M.; Wang, J.; Jin, G.; Jiang, Y.; Zhang, X.; Liu, X.; Chu, P. K. In vitro and in vivo Anti-biofilm Effects of Silver Nanoparticles Immobilized on Titanium. *Biomaterials* **2014**, *35*, 9114−9125.

(11) Agarwal, A.; Weis, T. L.; Schurr, M. J.; Faith, N. G.; Czuprynski, C. J.; McAnulty, J. F.; Murphy, C. J.; Abbott, N. L. Surfaces Modified with Nanometer-thick Silver-impregnated Polymeric Films that Kill Bacteria But Support Growth of Mammalian Cells. *Biomaterials* **2010**, *31*, 680−690.

(12) Besinis, A.; De Peralta, T.; Handy, R. D. Inhibition of Biofilm Formation and Antibacterial Properties of a Silver Nano-coating on Human Dentine. *Nanotoxicology* **2014**, *8*, 745−754.

(13) Rai, M.; Yadav, A.; Gade, A. Silver Nanoparticles as a New Generation of Antimicrobials. *Biotechnol. Adv.* **2009**, *27*, 76−83.

(14) Chen, X.; Schluesener, H. J. Nanosilver: a Nanoproduct in Medical Application. *Toxicol. Lett.* **2008**, *176*, 1−12.

(15) Qin, H.; Zhu, C.; An, Z.; Jiang, Y.; Zhao, Y.; Wang, J.; Liu, X.; Hui, B.; Zhang, X.; Wang, Y. Silver Nanoparticles Promote Osteogenic Differentiation of Human Urine-derived Stem Cells at Noncytotoxic Concentrations. *Int. J. Nanomed.* **2014**, *9*, 2469−2478.

(16) Braydich-Stolle, L.; Hussain, S.; Schlager, J. J.; Hofmann, M. C. In vitro Cytotoxicity of Nanoparticles in Mammalian Germline Stem Cells. *Toxicol. Sci.* **2005**, *88*, 412−419.

(17) Samberg, M. E.; Loboa, E. G.; Oldenburg, S. J.; Monteiro-Riviere, N. A. Silver Nanoparticles Do Not Influence Stem Cell Differentiation but Cause Minimal Toxicity. *Nanomedicine (London, U. K.)* **2012**, *7*, 1197−1209.

(18) Park, E. J.; Yi, J.; Kim, Y.; Choi, K.; Park, K. Silver Nanoparticles Induce Cytotoxicity by a Trojan-horse Type Mechanism. *Toxicol. In Vitro* **2010**, *24*, 872−878.

(19) Cao, H.; Qiao, Y.; Liu, X.; Lu, T.; Cui, T.; Meng, F.; Chu, P. K. Electron Storage Mediated Dark Antibacterial Action of Bound Silver Nanoparticles: Smaller Is Not Always Better. *Acta Biomater.* **2013**, *9*, 5100−5110.

(20) Cao, H.; Liu, X.; Meng, F.; Chu, P. K. Biological Actions of Silver Nanoparticles Embedded in Titanium Controlled by Micro-galvanic Effects. *Biomaterials* **2011**, *32*, 693−705.

(21) Fiedler, J.; Kolitsch, A.; Kleffner, B.; Henke, D.; Stenger, S.; Brenner, R. E. Copper and Silver Ion Implantation of Aluminium Oxide-blasted Titanium Surfaces: Proliferative Response of Osteoblasts and Antibacterial Effects. *Int. J. Artif. Organs* **2011**, *34*, 882−888.

(22) Han, Y.; Chen, D.; Sun, J.; Zhang, Y.; Xu, K. UV-enhanced Bioactivity and Cell Response of Micro-arc Oxidized Titania Coatings. *Acta Biomater.* **2008**, *4*, 1518−1529.

(23) Huo, K.; Zhang, X.; Wang, H.; Zhao, L.; Liu, X.; Chu, P. K. Osteogenic Activity and Antibacterial Effects on Titanium Surfaces Modified with Zn-incorporated Nanotube Arrays. *Biomaterials* **2013**, *34*, 3467−3478.

(24) Qin, H.; Zhao, Y.; Cheng, M.; Wang, Q.; Wang, Q.; Wang, J.; Jiang, Y.; An, Z.; Zhang, X. Anti-biofilm Properties of Magnesium Metal via Alkaline PH. *RSC Adv.* **2015**, *5*, 21434−21444.

(25) An, Y. H.; Friedman, R. J. Animal Models of Orthopedic Implant Infection. *J. Invest. Surg.* **1998**, *11*, 139−146.

(26) Cai, K.; Frant, M.; Bossert, J.; Hildebrand, G.; Liefeith, K.; Jandt, K. D. Surface Functionalized Titanium Thin Films: Zeta-potential, Protein Adsorption and Cell Proliferation. *Colloids Surf., B* **2006**, *50*, 1−8.

(27) Wang, W.; Ouyang, Y.; Poh, C. K. Orthopaedic Implant Technology: Biomaterials from Past to Future. *Ann. Acad. Med. Singapore* **2011**, *40*, 237−244.

DOI: 10.1021/acsami.5b01310
ACS Appl. Mater. Interfaces 2015, 7, 10785−10794

(28) McBeath, R.; Pirone, D. M.; Nelson, C. M.; Bhadriraju, K.; Chen, C. S. Cell Shape, Cytoskeletal Tension, and RhoA Regulate Stem Cell Lineage Commitment. *Dev. Cell* **2004**, *6*, 483−495.
(29) Zhao, L.; Wang, H.; Huo, K.; Zhang, X.; Wang, W.; Zhang, Y.; Wu, Z.; Chu, P. K. The Osteogenic Activity of Strontium Loaded Titania Nanotube Arrays on Titanium Substrates. *Biomaterials* **2013**, *34*, 19−29.
(30) Wang, C.; Lin, K.; Chang, J.; Sun, J. Osteogenesis and Angiogenesis Induced by Porous Beta-CaSiO(3)/PDLGA Composite Scaffold via Activation of AMPK/ERK1/2 and PI3K/Akt Pathways. *Biomaterials* **2013**, *34*, 64−77.
(31) Ge, C.; Xiao, G.; Jiang, D.; Franceschi, R. T. Critical Role of the Extracellular Signal-regulated Kinase-MAPK Pathway in Osteoblast Differentiation and Skeletal Development. *J. Cell Biol.* **2007**, *176*, 709−718.
(32) Khatiwala, C. B.; Kim, P. D.; Peyton, S. R.; Putnam, A. J. ECM Compliance Regulates Osteogenesis by Influencing MAPK Signaling Downstream of RhoA and ROCK. *J. Bone Miner. Res.* **2009**, *24*, 886−898.

DOI: 10.1021/acsami.5b01310
ACS Appl. Mater. Interfaces 2015, 7, 10785−10794